analytical chemistry

pubs.acs.org/ac Article

Reversible Ratiometric Electrochemiluminescence Biosensor Based on DNAzyme Regulated Resonance Energy Transfer for Myocardial miRNA Detection

Yudie Sun, La Fang, Yunxiang Han, Aobo Feng, Shengjun Liu, Kui Zhang,* and Jing-Juan Xu

Cite This: *Anal. Chem.* 2022, 94, 7035−7040 Read Online

ACCESS | Metrics & More | Article Recommendations | Supporting Information

ABSTRACT: Myocardial miRNAs in peripheral blood are closely related to the pathogenic process of myocardial infarction. Rapid identification and accurate quantification of myocardial miRNAs are of great significance to clinical interventions for treating cardiovascular lesions. Therefore, a ratiometric electrochemiluminescence (ECL) biosensor integrating DNAzyme with a resonance energy transfer (RET) system was designed to detect myocardial miRNA. The dual-signal system was composed of rA marked substrate strand functionalized CdTe quantum dots (QDs) as reductive−oxidative (R−O) emitters and Cy5-labeled strand-functionalized $Ru(bpy)_3^{2+}$-filled silica nanoparticles (RuSi NPs) as oxidative−reductive (O−R) emitters. In the presence of target miRNA, DNAzyme was activated to cut substrate strands on the CdTe QDs and release triggers for opening hairpin probes. Then, the Cy5 molecule-labeled hairpin DNA on the RuSi NPs was opened to introduce Cy5 molecules and RuSi NPs into the system. The R−O ECL was quenched by ECL-RET between CdTe QDs and Cy5 molecules and the O−R ECL was introduced by the RuSi NPs. In this way, based on the simultaneous changing of the ECL signal, the dual-potential dynamic signal ratiometric ECL sensing platform was developed. By measuring the ratio of O−R ECL signal to R−O ECL signal, the concentration of miRNA-499 was accurately quantified in the range of 10 fM to 10 nM, and the detection limit was as low as 2.44 fM ($S/N = 3$). This DNAzyme guided dual-potential ratiometric ECL method provides a sensitive and reliable method for myocardial miRNA detection, and it has great potential in clinical diagnosis and treatment.

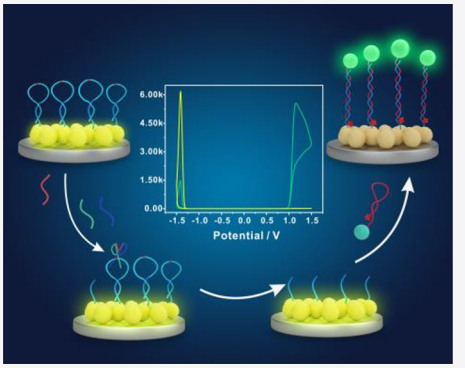

INTRODUCTION

Acute myocardial infarction (AMI) is a coronary syndrome characterized by acute and persistent hypoxic-ischemic myocardial damage, and it causes many deaths.[1,2] After the onset of AMI symptoms, the level of specific miRNA in peripheral blood increases significantly and then returns to the average level within a few hours.[3−6] Myocardial miRNA is considered to be a useful AMI biomarker due to its close correlation with cardiac myocytes and its stable presence in the circulatory system.[7] Therefore, the specific and sensitive detection of myocardial miRNA is of great significance for studying the pathogenesis of AMI and developing new diagnostic methods.[8,9]

To date, much progress has been made toward analyzing myocardial miRNA with various spectral technologies, including the catalytic hairpin assembly (CHA) triggered SERS detection strategy,[10,11] the DNAzyme-catalyzed electrochemiluminescence (ECL) method,[2,12] and point-of-care detection based on chemiluminescence.[13,14] Among these spectral techniques, ECL has attracted extensive attention for myocardial miRNA detection due to its high sensitivity, wide detection range, and controllable potential.[15,16] However, false signals often appear during ECL analysis due to interference from the instruments involved and the environment, and these false signals affect the intensity of detectable signals.[17] Theoretically, ECL analysis based on the ratio of two different potential values can calibrate most deviations and improve the reliability of the detection results. Therefore, ratiometric ECL strategies are well suited for detecting miRNA in peripheral blood and will further promote the application of ECL in the clinical diagnosis and treatment of AMI.[18,19]

To improve the sensitivity of ECL biosensors for miRNA detection, numerous amplification technologies and nanomaterials have been integrated with ECL technology. For example, CHA,[20−22] rolling circle amplification,[23,24] and hybridization chain reaction[25−28] have been combined with luminescent materials for miRNA detection or imaging. Among these amplification technologies, DNAzyme, a metal-ion-dependent enzyme structure composed of nucleic acids,

Received: January 13, 2022
Accepted: April 15, 2022
Published: April 25, 2022

https://doi.org/10.1021/acs.analchem.2c00195
Anal. Chem. 2022, 94, 7035−7040

has shown excellent catalytic activity and high specificity.[29−34] By modifying ribo-adenine (rA) sites and properly designing the base structure, the base can be cleaved to release the required sequence. As a sensitive component of signal amplification, DNAzyme can significantly improve the performance of ECL sensors and further expand the application of ECL.

Actually, the advances in ECL methods for myocardial miRNA detection have heavily relied on the design of suitable amplification strategy and the development of reliable signal calibration method. In this work, a ratiometric ECL-sensing platform was developed to detect myocardial miRNA based on DNAzyme guided dual-potential emission. As shown in Scheme 1, CdTe quantum dots (QDs) were chosen as

Scheme 1. Schematic Diagram of This ECL Strategy for Myocardial miRNA Detection

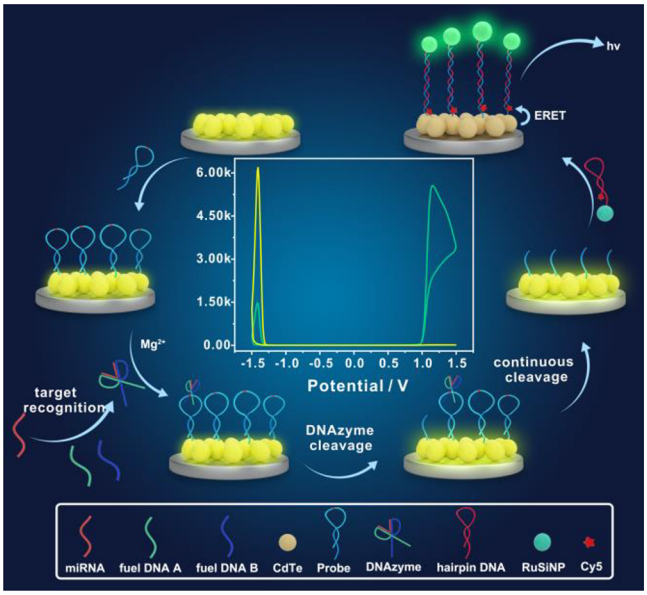

reductive−oxidative (R−O) emitters, and RuSi nanoparticles (NPs) modified by hairpin DNA and quenching agent Cy5 molecules were used as oxidative−reductive (O-R) emitters. A layer of CdTe QDs film was coated on a glassy carbon electrode (GCE), which generated a very strong initial ECL signal at negative potential. Then, the probe was anchored on the film through NH_2 bonding. In the presence of target miRNA, two well-designed fuel chains (fuel DNA A and fuel DNA B) can specifically bind to target miRNA, and form a cleavage cycle amplification unit as part of DNAzyme. Then, under the activation of magnesium ions, the Mg^{2+}-dependent DNAzyme was activated and the substrate strand with rA sites on CdTe QDs was sheared continuously. Subsequently, the cleaved product triggered the opening of Cy5-labeled hairpin DNA on RuSi NPs, which brought Cy5 close to the CdTe QDs. As a result, the R−O ECL signal was quenched by ECL-resonance energy transfer (ECL-RET) between the CdTe QDs and Cy5 molecules, whereas the O−R ECL signal at positive potential was enhanced by the RuSi NPs. Based on the ratio of the two competing ECL signals, this method showed good performance in detecting myocardial miRNA in serum. The DNAzyme guided ratiometric ECL strategy improves the reliability of blood sample detection and promises to extend the application of ECL in disease diagnosis.

EXPERIMENTAL SECTION

Materials and Reagents. All qualified auxiliary DNA was purchased from Sangon Biotechnology. Myocardial miRNA (miRNA-499) and other miRNAs were purified by Gemma Pharma. Table S1 lists the gene sequences relevant to this work. Polyacrylamide, Tris, and RNase inhibitors were also purchased from Sangon Biotechnology. Tris(2,2′-bipyridyl) ruthenium(II) chloride hexahydrate [$Ru(bpy)_3Cl_2·6H_2O$], tripropylamine (TPA), (3-aminopropyl)-triethoxysilane (APTES), cadmium chloride hydrate ($CdCl_2·2.5H_2O$), tetraethyl orthosilicate (TEOS), amino polyethylene glycol (PEG), and thiourea were purchased from Shanghai Aladdin Corporation (Shanghai, China). Potassium peroxydisulfate ($K_2S_2O_8$), magnesium acetate ($MgAC_2$), triton X-100, cyclohexane, ammonia solution (NH_4OH, 25%), and 1-hexanol were obtained from Sinopharm Corporation. All chemicals were of at least analytical grade.

Instrumentation. A MPI-B-type multiparameter chemical analysis and testing system from Xi'an Reman Electronic Science and Technology Company (Xi'an, China) was used for ECL measurements. The CdTe QDs and RuSi NPs were characterized by a JEM-2100 transmission electron microscope (TEM) with a voltage bias of 600 V and a scanning rate of 0.1 $V·s^{-1}$.

Polyacrylamide Gel Electrophoresis (PAGE). All DNA was annealed at 95 °C for 10 min and then gradually cooled to room temperature for standby. Varying concentrations of miRNA-499 were mixed with 20 μL of TA buffer, which contained 0.1 μM fuel A, 0.1 μM fuel B, and 0.1 μM probe, and then each mixture was incubated at 37 °C for 3 h to produce the DNAzyme digestion product. Electrophoresis for DNAzyme was carried out by 12% PAGE (w/w) for 10 h (96 V, 4 °C). First, prepare 12% polyacrylamide gel and pour the prepared gel into the gel bed between the two glass plates. Then, gently insert a suitable size of the comb to the upper edge of the short glass plate. After the gel is formed, take out the comb carefully and rinse the sample adding hole with buffer immediately. Next, the gel was fixed on the electrophoresis tank, and 1× TBE buffer was added. The DNA sample was mixed with an appropriate amount of loading buffer, and then added to the sample well. Subsequently, electrodes were connected for electrophoresis. Finally, the gel was immersed in the dyeing solution for 30 min. The results were observed under UV and photographed in the gel imaging system.

Synthesis of CdTe QDs. The CdTe QDs were synthesized according to previous literature.[35] First, 0.2284 g of $CdCl_2·2.5H_2O$ was dissolved in 125 mL of ultrapure water. Next, 210 μL of MPA was added to the solution, and the pH was adjusted to 11. The mixture was protected under nitrogen for 30 min. Then, 8 mL of 0.5 M H_2SO_4 was injected into the mixed solution with a needle. After being refluxed at 170 °C for 12 h, the mixed solution was refluxed at 120 °C for 11 h. The synthesized CdTe QDs were dialyzed with deionized water overnight. Finally, the purified product was kept at 4 °C for later use.

Synthesis and Modification of the RuSi NPs. According to previous literature for preparing RuSi NPs,[36,37] 340 μL of $Ru(bpy)_3^{2+}$ (40 mmol/L), 1.77 mL of Triton X-100, 7.5 mL of cyclohexane, and 1.8 mL of 1-hexanol were mixed and stirred for 20 min to form a microemulsion. Then, 60 μL of NH_4OH and 100 μL of TEOS were added into the mixed solution and

https://doi.org/10.1021/acs.analchem.2c00195
Anal. Chem. 2022, 94, 7035−7040

reacted for 24 h. Next, the emulsion was destroyed with acetone, and then washed several times. Then the obtained solution was soaked in APTES to obtain amino-functionalized RuSi NPs. Unreacted APTES was washed with ethanol and water by centrifugation, and the amino-functionalized RuSi NPs were redispersed in 500 μL of ultrapure water. Then, 200 μL of RuSi NPs and 3 μM of hairpin DNA were added to 1 mL of PBS buffer (pH 7.4) that contained 20 mM EDC and 10 mM NHS. The mixtures were incubated in darkness for 5 h under shaking. Finally, the mixture was centrifugally washed and redispersed in PBS buffer.

Fabrication of the ECL Biosensor. The GCE was polished to obtain a mirror surface, it was ultrasonically cleaned and dried in air. For the cathode emission, 10 μL of the CdTe QDs solution was dropped onto the pretreated GCE and evaporated in air to obtain a CdTe QDs membrane. To prevent the CdTe QDs from falling off, 5 μL 0.1% naphthol was added dropwise and dried naturally. Then, the CdTe QD-modified GCE was immersed in 10 mM Tris−HCl buffer (pH 7.4) that contained 20 mM EDC and 10 mM NHS for 1 h at room temperature to carboxylate the QDs on the electrode surface. After washing with Tris−HCl buffer, the probe was modified on the electrode by dropping 10 μL of 3.0 μM probe DNA onto the electrode for 3 h. Subsequently, amino PEG was added to prevent nonspecific binding, since it can bond onto the surface of CdTe QDs by the linkage of amino groups with the activated carboxyl groups of CdTe QDs, and a PEG chain possesses low affinity for various biomacromolecules.[38,39] Finally, target miRNA was mixed with 10 μL of 3.0 μM fuel A and 3.0 μM fuel B, and the resulting solution was incubated for 2 h to complete continuous cutting. After the reaction, the electrode surface was slowly washed with PBS buffer to remove excess nucleic acid. Subsequently, 10 μL of hairpin DNA-modified RuSi NPs was dropped onto the surface of the GCE containing the cleavage product, and then the electrode was incubated at 37 °C in darkness for 3 h. After that, the electrode was thoroughly washed to remove unreacted NPs. ECL characterization was performed in PBS buffer containing 25 mM TPA and 0.1 M $K_2S_2O_8$ to verify the success of each step of the reaction process. As shown in Figure S1, the concentration of TPA and $K_2S_2O_8$ was also optimized.

RESULTS AND DISCUSSION

Characterization of CdTe QDs and RuSi NPs. RuSi NPs and CdTe QDs were applied as two different ECL emitters for ratiometric ECL detection of miRNA. The morphologies of the prepared CdTe QDs and RuSi NPs were characterized by TEM images. Moreover, the average hydrodynamic sizes of the CdTe QDs and RuSi NPs were determined by dynamic light scattering (DLS). Figure 1A,B illustrates the homogeneous morphologies of the CdTe QDs and RuSi NPs. Figure 1C,D shows a good dispersion of CdTe QDs and RuSi NPs with average diameters of 2.49 and 52.21 nm, respectively. The successful modification of hairpin DNA on RuSi NPs was confirmed by DLS analysis and zeta potential measurement (Figure S2). Element mapping analysis was performed to characterize the element distribution of the RuSi NPs. As expected, the main elements of the RuSi NPs were oxygen, silicon, and ruthenium, which were distributed evenly in the spherical NPs. The TEM energy-dispersive spectrum of the RuSi NPs revealed the weight ratio of Ru:O:Si was 1:28.6:23.1 (Figure S3). These results indicated that $Ru(bpy)_3^{2+}$ was effectively doped into SiO_2, which was beneficial for enhancing

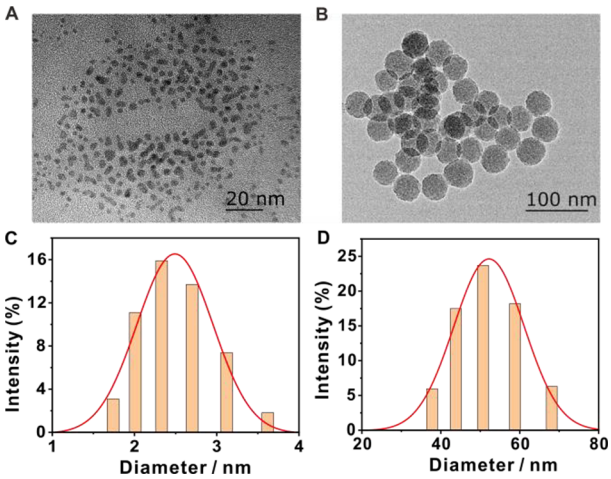

Figure 1. TEM images of (A) CdTe QDs and (B) RuSi NPs. DLS images of (C) CdTe QDs and (D) RuSi NPs.

the anode ECL signal. Although the content of Ru is relatively small, the increase in the number of $Ru(bpy)_3^{2+}$ molecules in per nanoparticle contributes greatly to the signal enhancement of ECL.

Feasibility and Characteristics of the Ratiometric ECL Biosensor. To confirm the formation of DNAzyme and the successful hybridization with hairpin DNA, the structures were characterized by PAGE. PAGE is the most often used technique in nucleic acid analysis. It is based on the principle that nucleic acids can migrate toward the anode under electric field, since they are negatively charged. As mass is proportional to charge, the gel can selectively impede the migration of nucleic acid structures in proportion to its chain length and topology. From Figure 2A, the mixture of miRNA-499, fuel A,

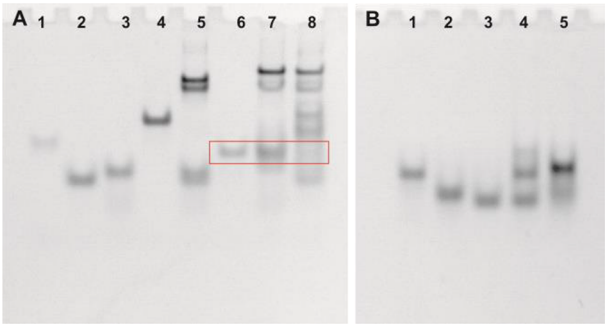

Figure 2. (A) Analysis of DNAzyme (12% PAGE). Lane 1: miRNA-499; Lane 2: fuel A; Lane 3: fuel B; Lane 4: probe; Lane 5: mixture of fuel A, fuel B, and probe; Lane 6: the cleavage product; Lane 7: mixture of miRNA-499, fuel A, fuel B, and probe (with rA site); Lane 8: mixture of miRNA-499, fuel A, fuel B, and probe similar structure without rA site. (B) Analysis of the assembly with hairpin DNA (6% PAGE). Lane 1: probe; Lane 2: the cleavage product; Lane 3: hairpin DNA; Lane 4: probe and hairpin DNA; Lane 5: the cleavage product and hairpin DNA.

and fuel B showed new bands of the monomer (lane 5), illustrating the successful assembly of the cyclic units. By comparing the bands in lane 7 with those in lane 8, a new band in lane 7 corresponding to the product chain cut by DNAzyme indicated the successful cleavage of the probe. From Figure 2B, the mixture of the probe and hairpin DNA showed the defined bands of DNA monomers (lane 4), suggesting that the two

https://doi.org/10.1021/acs.analchem.2c00195
Anal. Chem. 2022, 94, 7035−7040

well-designed hairpin DNA structures could coexist stably. ECL measurements also confirmed that HP could not open the probe DNA and had no influence for the probe DNA (Figure S4). The above results showed the successful nucleic acid amplification process, which reflected the good probe design.

The fabrication steps of the biosensor were monitored by cyclic voltammetry (CV) and electrochemical impedance spectroscopy (EIS). In addition, the electrochemical process was simulated by equivalent circuit of impedance analysis (the inset of Figure 3B), and the Nyquist diagram's high-frequency

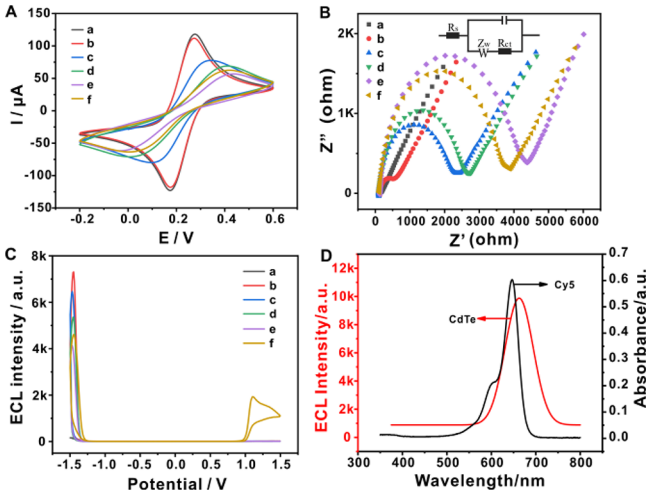

Figure 3. Characterization of biosensors with stepwise fabrications based on (A) CV curves, (B) EIS curves, and (C) ECL potential spectra. Regarding the legends in (a)−(f): GCE, CdTe/GCE, probe/CdTe/GCE, PEG/probe/CdTe/GCE, DNAzyme/PEG/probe/CdTe/GCE, and RuSiNP-S2-HP/DNAzyme/PEG/probe/CdTe/GCE with target. (D) ECL emission spectrum of CdTe QDs and UV absorption spectrum of Cy5 in aqueous solution.

semicircles directly reflected the resistance of the charge transfer (R_{ct}). As shown in Figure 3A,B, the measurement results of the bare GCE showed a couple quasi-reversible redox peaks of $[Fe(CN)_6]^{3-/4-}$ and a very narrow semicircle (curve a). The redox peak current of CdTe/GCE was reduced and the resistance of charge transfer (R_{ct}) of the bare electrode was enhanced because the film prevented electron transport (curve b). As the probe and sealing agent were fixed sequentially, the peak current gradually decreased and R_{ct} further increased (curves c and d), because electron transport was further prevented. After adding the target miRNA, fuel A, and fuel B, a composite structure was formed on the electrode surface, which made the electrode surface have more negative charges, resulting in a decrease in the redox current and a significant increase in R_{ct} (curve e). Then, hairpin DNA modified RuSi NPs were incubated on the electrode surface, and the negative charge decreased due to the transformation of structures from a composite structure to a double-chain structure, resulting in a significant increase in redox current and decrease in resistance (curve f).[40]

In addition, ECL analysis was also performed to study the ECL spectrum in the manufacturing process of the ratiometric ECL sensor. From Figure 3C, no obvious ECL response signal was observed on the bare electrode (curve a), whereas an original ECL signal with a high intensity was observed at −1.5 V when CdTe QDs were fixed on the GCE surface (curve b). Then, after the step-by-step assembly of the probe, PEG, and DNAzyme (curves c−d), the ECL signal of the CdTe QDs decreased gradually. Subsequently, when hairpin DNA modified RuSiNPs were incubated on the DNAzyme/PEG/probe/CdTe/GCE electrode, a new ECL signal appeared at 1.0 V; meanwhile, the ECL signal at −1.5 V decreased significantly, which was due to the energy resonance of Cy5 and CdTe QDs.

ECL-RET technology has received extensive attention in the development of biosensors. The key to RET is that the ECL spectrum of the donor overlaps with the UV−vis absorption spectrum of the receptor.[41,42] To study the ECL-RET mechanism, the UV absorption spectrum of Cy5 and the ECL emission of CdTe QDs were obtained (Figure 3D). Cy5 had an obvious absorption peak at approximately 648 nm, and CdTe QDs had an ECL emission peak centered at 647 nm. The ECL emission of CdTe QDs overlapped significantly with the absorption spectrum of Cy5. Besides, an excitonic emission peak of CdTe QDs centered at 622 nm was observed in fluorescence spectrum (Figure S5). The PL emission of CdTe QDs also prominently overlaps with the absorption spectrum of Cy5. The above experimental results indicate that effective ECL-RET can be carried out from the CdTe QDs to Cy5.

ECL Analysis of Myocardial miRNA. In order to obtain the optimal experimental performance, the concentration of Cy5, the incubation time of DNAzyme, and the concentration of Mg^{2+} in the reaction solution were analyzed (Figure S6). The concentration of Cy5 was critical to the performance of the biosensor. The ECL signal gradually increased with an increasing concentration of Cy5 and reached a maximum at 3 μM. Therefore, the optimal concentration of Cy5 was 3 μM in this work. The reaction time of DNAzyme after the reaction solution was dropped on the proposed electrode was also discussed. The ratio of anode signal intensity to cathode ECL intensity gradually increased with increasing reaction time, and a stable ECL intensity was achieved in 3 h, which was selected as the optimal reaction time. Moreover, 10 mM was selected as the concentration of Mg^{2+} for the experiment.

Under optimal conditions, the effective ratiometric ECL-RET system between the CdTe QDs and RuSi NPs was used to sensitively detect miRNA-499 at different concentrations (Figure 4A). The ECL at the negative potential of the CdTe QDs decreased with the increase in target concentration, and the ECL at the positive potential of the RuSi NPs increased accordingly (Figure 4B). To make the results more reliable, the ratio method was used to detect the target miRNA. As shown in Figure 4C, the logarithm of the ratio of anode to cathode ECL peak intensity (I_a/I_c) was linearly dependent on the logarithm of the target concentration in the range of 10 nM to 10 fM, and the correlation coefficient was 0.995. The relationship between the concentration and intensity of miRNA-499 was calibrated from 10 fM to 10 nM with a limit of detection of 2.44 fM (S/N = 3).

To verify the clinical effect, miRNA-499 in real serum samples was detected. When comparing the ECL results in 10% human serum with that in buffer (Figure 4D), no significant differences in intensity or potential were found. In 10% human serum, the peak intensity of R−O ECL decreased with the increase in target concentration, whereas the intensity of O−R ECL increased (Figure 4E). The quantitative detection results in actual samples were consistent with those in buffer (Figure 4F). Therefore, the ratiometric ECL detection strategy can be applied in actual samples and has great potential in the diagnosis of AMI.

https://doi.org/10.1021/acs.analchem.2c00195
Anal. Chem. 2022, 94, 7035−7040

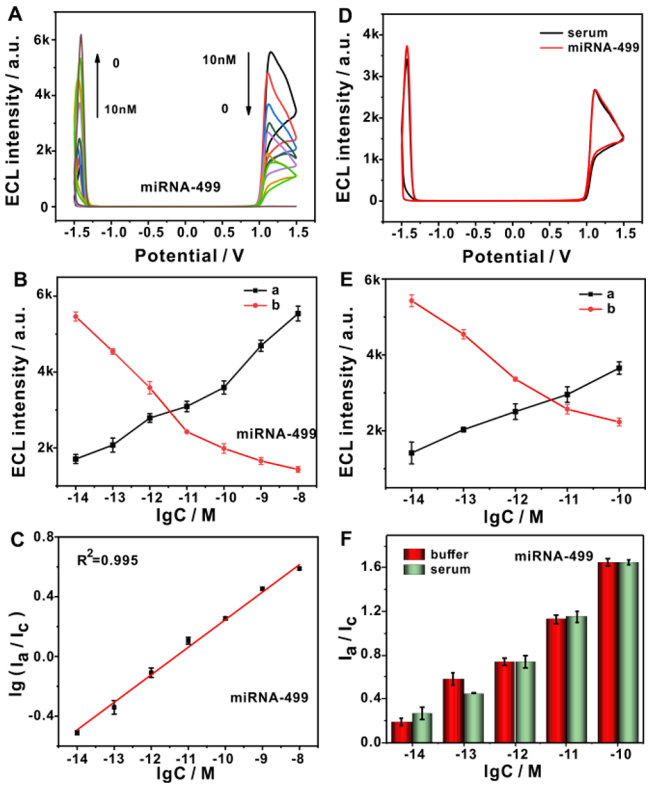

Figure 4. (A) ECL intensity at different concentrations of miRNA-499 (10 fM to 10 nM). (B) Relationship between the ECL intensity of (a) RuSi NPs or (b) CdTe QDs and the logarithm of the concentration of miRNA-499 in the range of 10 fM to 10 nM. (C) Relationship between the ratio of ECL signal at anode (RuSi NPs) to ECL signal at cathode (CdTe QDs) and the concentration of miRNA-499. (D) ECL intensity−potential curves for detection of 10 pM miRNA-499 in buffer and in 10% serum. (E) Relationship between the ECL intensity of (a) RuSi NPs or (b) CdTe QDs and the logarithmic of the concentration of miRNA-499 in the range of 10 fM to 10 pM. (F) Comparison of the detection results of myocardial miRNA in TE buffer and in 10% serum.

Stability and Specificity of the ECL Biosensor. Stability is a key parameter for evaluating the behavior of ECL-RET biosensors. To judge whether the performance of the biosensor was stable under multiple cycles of scanning, the constructed biosensor was scanned under a continuous potential with 1 fM of miRNA-499. As Figure 5A shows, both ECL signals maintained almost no obvious decay (RSD_a = 2.8%/RSD_c = 4.5%) under consecutive potential scans for 10 cycles, indicating the practicability for ECL detection. Selectivity is another important indicator for evaluating the successful construction of ECL biosensors. To evaluate the specificity of the analysis, miRNA-208, miRNA-328, miRNA-21, miRNA-499, and a mixture of all the miRNAs were detected. The results of comparative experiments show that 10 pM target could trigger distinguishable changes in ECL signal, and the signal corresponding to control groups was almost the same as the blank signal, even at higher concentrations. In addition, for the mixed sample, detectable signals appear to be caused only by miRNA-499 (Figure 5B). The experimental results successfully proved that the above biosensor has high selectivity and can be used for the detection of myocardial miRNA.

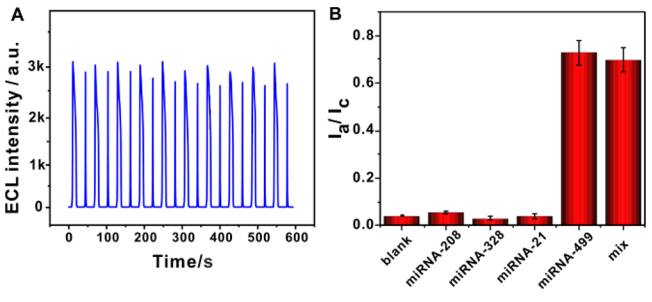

Figure 5. (A) Stability of ECL biosensor of RuSi NPs (0dd circle) and CdTe QDs (even circle) under continuous cyclic potential scans for 10 cycles. (B) ECL of the present ECL biosensor in blank, 10 nM of miRNA-208, 10 nM of miRNA-328, 10 nM of miRNA-21, 10 pM of miRNA-499, and a mixture of all the miRNAs.

CONCLUSIONS

In summary, an efficient ratiometric ECL system was designed based on DNAzyme-guided ECL-RET between CdTe QDs and Cy5 on RuSi NPs for the reliable analysis of myocardial miRNA. CdTe QDs and RuSi NPs on the electrode exhibited a stable and strong ECL signal in the presence of coreactant $S_2O_8^{2-}$ and TPA, implying good potential in myocardia miRNA detection. With the increase in target miRNA, the ECL intensity of CdTe QDs decreased, whereas that of RuSi NPs enhanced gradually, suggesting that the ratiometric ECL-RET design was effective. The proposed ECL-RET system is expected to open new avenues for processing dual-potential ECL ratiometric assays for clinical diagnosis and real-time monitoring of myocardial infarction.

ASSOCIATED CONTENT

Supporting Information

The Supporting Information is available free of charge at https://pubs.acs.org/doi/10.1021/acs.analchem.2c00195.

The HAADF image for RuSi NPs, FT-IR spectra of RuSi NPs, RuSi NPs-NH2, and RuSiNP-CONH-DNA-Cy5, and table of all used gene sequences (DOCX)

AUTHOR INFORMATION

Corresponding Author

Kui Zhang − *School of Chemistry and Chemical Engineering, Anhui University of Technology, Ma 'anshan, Anhui 243032, People's Republic of China;* orcid.org/0000-0002-5634-9952; Email: zhangkui@mail.ustc.edu.cn

Authors

Yudie Sun − *School of Chemistry and Chemical Engineering, Anhui University of Technology, Ma 'anshan, Anhui 243032, People's Republic of China;* orcid.org/0000-0002-1053-7472

La Fang − *School of Chemistry and Chemical Engineering, Anhui University of Technology, Ma 'anshan, Anhui 243032, People's Republic of China*

Yunxiang Han − *School of Chemistry and Chemical Engineering, Anhui University of Technology, Ma 'anshan, Anhui 243032, People's Republic of China*

Aobo Feng − *School of Chemistry and Chemical Engineering, Anhui University of Technology, Ma 'anshan, Anhui 243032, People's Republic of China*

https://doi.org/10.1021/acs.analchem.2c00195
Anal. Chem. 2022, 94, 7035−7040

Shengjun Liu − *School of Chemistry and Chemical Engineering, Anhui University of Technology, Ma 'anshan, Anhui 243032, People's Republic of China*

Jing-Juan Xu − *State Key Laboratory of Analytical Chemistry for Life Science, School of Chemistry and Chemical Engineering, Nanjing University, Nanjing 210023, People's Republic of China;* orcid.org/0000-0001-9579-9318

Complete contact information is available at: https://pubs.acs.org/10.1021/acs.analchem.2c00195

Notes

The authors declare no competing financial interest.

■ ACKNOWLEDGMENTS

This work was supported by the National Natural Science Foundation of China (Nos. 22004003 and 62104003).

■ REFERENCES

(1) van Rooij, E.; Sutherland, L. B.; Thatcher, J. E.; DiMaio, J. M.; Naseem, R. H.; Marshall, W. S.; Hill, J. A.; Olson, E. N. *Proc. Natl. Acad. Sci. U S A* **2008**, *105*, 13027−13032.
(2) Sun, Y.; Wang, Q.; Mi, L.; Shi, L.; Li, T. *Anal. Chem.* **2019**, *91*, 12948−12953.
(3) Fiedler, J.; Thum, T. *Arterioscler. Thromb. Vasc. Biol.* **2013**, *33*, 201−205.
(4) Chen, Z.; Miao, L.; Liu, Y.; Dong, T.; Ma, X.; Guan, X.; Zhou, G.; Zou, B. *Chem. Commun. (Camb)* **2017**, *53*, 12922−12925.
(5) Ottersbach, A.; Mykhaylyk, O.; Heidsieck, A.; Eberbeck, D.; Rieck, S.; Zimmermann, K.; Breitbach, M.; Engelbrecht, B.; Brugmann, T.; Hesse, M.; et al. *Biomaterials* **2018**, *155*, 176−190.
(6) Sun, T.; Dong, Y. H.; Du, W.; Shi, C. Y.; Wang, K.; Tariq, M. A.; Wang, J. X.; Li, P. F. *Int. J. Mol. Sci.* **2017**, *18*, 745.
(7) Wang, X.; Tian, L.; Sun, Q. *J. Clin. Lab. Anal.* **2020**, *34*, 2410−2417.
(8) Dong, H.; Lei, J.; Ding, L.; Wen, Y.; Ju, H.; Zhang, X. *Chem. Rev.* **2013**, *113*, 6207−6233.
(9) Graybill, R. M.; Bailey, R. C. *Anal. Chem.* **2016**, *88*, 431−450.
(10) Sun, Y.; Li, T. *Anal. Chem.* **2018**, *90*, 11614−11621.
(11) Tian, L.; Su, M.; Yu, F.; Xu, Y.; Li, X.; Li, L.; Liu, H.; Tan, W. *Nat. Commun.* **2018**, *9*, 1−12.
(12) Sun, Y.; Fang, L.; Zhang, Z.; Yi, Y.; Liu, S.; Chen, Q.; Zhang, J.; Zhang, C.; He, L.; Zhang, K. *Anal. Chem.* **2021**, *93*, 7516−7522.
(13) Shi, L.; Sun, Y.; Mi, L.; Li, T. *ACS Sens.* **2019**, *4*, 3219−3226.
(14) Sun, Y.; Shi, L.; Wang, Q.; Mi, L.; Li, T. *Anal. Chem.* **2019**, *91*, 3652−3658.
(15) Liu, Z.; Qi, W.; Xu, G. *Chem. Soc. Rev.* **2015**, *44*, 3117−3142.
(16) Tan, X.; Zhang, B.; Zou, G. *J. Am. Chem. Soc.* **2017**, *139*, 8772−8776.
(17) Lee, M. H.; Kim, J. S.; Sessler, J. L. *Chem. Soc. Rev.* **2015**, *44*, 4185−4191.
(18) Guo, W.; Qiu, Z.; Guo, C.; Ding, D.; Li, T.; Wang, F.; Sun, J.; Zheng, N.; Liu, S. *ACS Appl. Mater. Interfaces* **2017**, *9*, 9348−9358.
(19) Huo, X. L.; Zhang, N.; Yang, H.; Xu, J. J.; Chen, H. Y. *Anal. Chem.* **2018**, *90*, 13723−13728.
(20) Huang, Q.; Ma, P.-Q.; Li, H.-D.; Yin, B.-C.; Ye, B.-C. *ACS Applied Bio Materials* **2020**, *3*, 2861−2866.
(21) Zhang, Y.; Chai, Y.; Wang, H.; Yuan, R. *Anal. Chem.* **2019**, *91*, 14368−14374.
(22) Zhu, L.; Zhang, M.; Ye, J.; Yan, M.; Zhu, Q.; Huang, J.; Yang, X. *Anal. Chem.* **2020**, *92*, 8614−8622.
(23) Chen, A.; Ma, S.; Zhuo, Y.; Chai, Y.; Yuan, R. *Anal. Chem.* **2016**, *88*, 3203−3210.
(24) Liu, C.; Han, J.; Zhou, L.; Zhang, J.; Du, J. *Sensors (Basel)* **2020**, *20*, 2017.
(25) Chen, J.; Yang, H.-H.; Yin, W.; Zhang, Y.; Ma, Y.; Chen, D.; Xu, Y.; Liu, S.-Y.; Zhang, L.; Dai, Z.; et al. *Anal. Chem.* **2019**, *91*, 4625−4631.
(26) Cheng, H.; Li, W.; Duan, S.; Peng, J.; Liu, J.; Ma, W.; Wang, H.; He, X.; Wang, K. *Anal. Chem.* **2019**, *91*, 10672−10678.
(27) Guo, Q.; Yu, Y.; Zhang, H.; Cai, C.; Shen, Q. *Anal. Chem.* **2020**, *92*, 5302−5310.
(28) Yin, F.; Liu, H.; Li, Q.; Gao, X.; Yin, Y.; Liu, D. *Anal. Chem.* **2016**, *88*, 4600−4604.
(29) Zhang, X.; Liu, H.; Li, R.; Zhang, N.; Xiong, Y.; Niu, S. *Chem. Commun.* **2015**, *51*, 6952−6955.
(30) Chen, J.; Zuehlke, A.; Deng, B.; Peng, H.; Hou, X.; Zhang, H. *Anal. Chem.* **2017**, *89*, 12888−12895.
(31) Cui, M. R.; Li, X. L.; Xu, J. J.; Chen, H. Y. *ACS Appl. Mater. Interfaces* **2020**, *12*, 13005−13012.
(32) Jiang, J.; Lin, X.; Diao, G. *ACS Appl. Mater. Interfaces* **2017**, *9*, 36688−36694.
(33) Li, P.; Wei, M.; Zhang, F.; Su, J.; Wei, W.; Zhang, Y.; Liu, S. *ACS Appl. Mater. Interfaces* **2018**, *10*, 43405−43410.
(34) Meng, X.; Zhang, K.; Yang, F.; Dai, W.; Lu, H.; Dong, H.; Zhang, X. *Anal. Chem.* **2020**, *92*, 8333−8339.
(35) Zhang, K.; Zhou, H.; Mei, Q.; Wang, S.; Guan, G.; Liu, R.; Zhang, J.; Zhang, Z. *J. Am. Chem. Soc.* **2011**, *133*, 8424−8427.
(36) Wang, Y. L.; Liu, F. R.; Cao, J. T.; Ren, S. W.; Liu, Y. M. *Biosens. Bioelectron.* **2018**, *102*, 525−530.
(37) Zhang, L.; Dong, S. *Anal. Chem.* **2006**, *78*, 5119−5123.
(38) Yoshimoto, K.; Nishio, M.; Sugasawa, H.; Nagasaki, Y. *J. Am. Chem. Soc.* **2010**, *132*, 7982−7989.
(39) Lakshmipriya, T.; Fujimaki, M.; Gopinath, S. C.; Awazu, K.; Horiguchi, Y.; Nagasaki, Y. *Analyst* **2013**, *138*, 2863−2870.
(40) Nie, Y.; Yuan, X.; Zhang, P.; Chai, Y. Q.; Yuan, R. *Anal. Chem.* **2019**, *91*, 3452−3458.
(41) Babamiri, B.; Salimi, A.; Hallaj, R. *Biosens. Bioelectron.* **2018**, *102*, 328−335.
(42) Li, J.; Li, D.; Yuan, R.; Xiang, Y. *ACS Appl. Mater. Interfaces* **2017**, *9*, 5717−5724.

https://doi.org/10.1021/acs.analchem.2c00195
Anal. Chem. 2022, 94, 7035−7040